

# Flux-Canceling Electrodynamic Maglev Suspension: Part II Test Results and Scaling Laws

Marc T. Thompson, *Member, IEEE*, and Richard D. Thornton, *Life Fellow, IEEE*

**Abstract**—Electrodynamic suspensions (EDS) are highly undamped and require some form of active control or a secondary suspension to achieve adequate ride quality. This paper reports on efforts to develop a version of EDS that uses controllable magnetic forces to eliminate the need for any secondary suspension. The magnetic forces act directly on the guideway and avoid the need to have unsprung weight and a secondary suspension. It is shown that the energy required to effect this control can be less than 1% of the energy stored in the suspension magnets, so a modest size controller can be used. The same controller can also provide lift at very low speeds and thereby eliminate the need for a separate low-speed suspension system. A set of scaling laws is described which is used to size a full-scale high-temperature superconductor (HTSC)-based suspension magnet. The test fixture was also used to verify the use of “zero velocity” lift, where ac excitation is used in the suspension coils to achieve lift at low train velocity.

**Index Terms**—Control systems, high-temperature superconductors, inductance, levitation, magnetic analysis, magnetic forces, magnetic levitation, maglev, modeling, superconducting coils, superconducting magnets.

## I. INTRODUCTION

THE design and analysis of a new iron-core “flux-canceling” magnetic suspension suitable for high-temperature superconductors (HTSC) is described. A 1/5-scale model of this suspension has been designed and tested with a high-speed rotating wheel test facility. A new low-cost multiple-loop guideway has been tested and lift, drag, and guidance forces have been measured at operating speeds approaching that of a full-scale train. These results are compared to predictions based on simple circuit models, with good results.

A vertical control system has been designed and tested to improve ride quality through differential control of the magnet currents. The test fixture has also been used to validate the concept of lift generation at zero train velocity by ac excitation of the main magnet coils. Scaling laws have been applied to the results and predictions made for a full-scale HTSC suspension operating at 40K. Further work in this area

may help overcome one of the fundamental limitations of electrodynamic (EDS) magnetic levitation (maglev)—the fact that there is zero levitation force at zero train velocity and a low speed suspension is needed.

## II. BASIC MAGLEV MEASUREMENTS

### A. Maglev Test Program

Details of the test fixture including speed control of the test wheel and operation of the data acquisition system are discussed in [1]–[4] and a companion paper in these TRANSACTIONS. The goals of the test program were as follows.

- Measure forces and moments for the magnets in different equilibrium positions and for different linear velocities using a multi-axis force sensor. Use the resultant data to verify models.
- Test the viability of using ac excitation of the magnet coils to achieve significant lift force at zero train velocity.
- Test the viability of actively controlled high temperature superconducting magnets in a magnetic secondary suspension by testing the magnet with a low-friction air bearing which allows vertical motion of the suspension magnet.

### B. Basic Measurements Using Force Sensor

The result of several test wheel runs is shown in Fig. 1 where the test wheel speed was varied from 0–600 RPM (linear speed, 0–50 m/s). In Fig. 1(a), the magnet was set below the null position, and a positive lift force is measured. In Fig. 1(b), the magnet was set +1.25 cm above the null position and a negative lift force is measured. The drag force shows a peak at approximately 20–25 m/s. Also of note is the guidance force, which is a significant fraction of the lift force. In Fig. 1(c), the magnet was set near the null position, and the lift and drag forces are minimized accordingly.

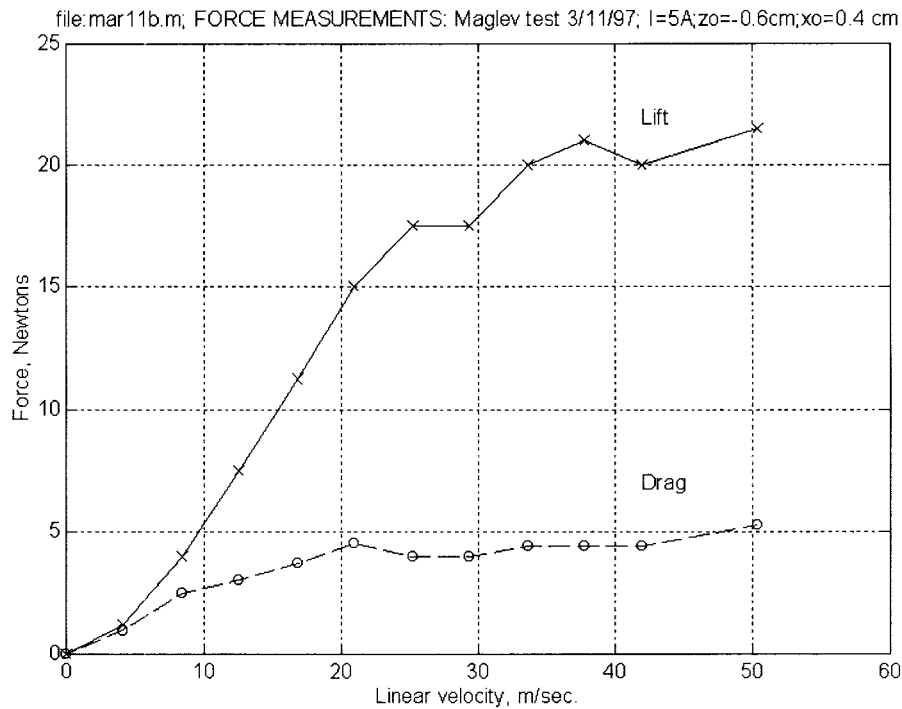
The important results from this test are that the drag peak velocity is approximately 20–25 m per second, which is significantly lower than the maximum test wheel speed. Therefore, data has been taken at speeds significantly higher than the drag peak velocity. This critical velocity will decrease significantly for a full-scale maglev magnet, shown with scaling laws developed later in this paper. Also, the guidance force for this configuration is a significant fraction of the lift force. This may enable a design without additional guidance coils.

Manuscript received June 3, 1998; revised January 11, 1999.

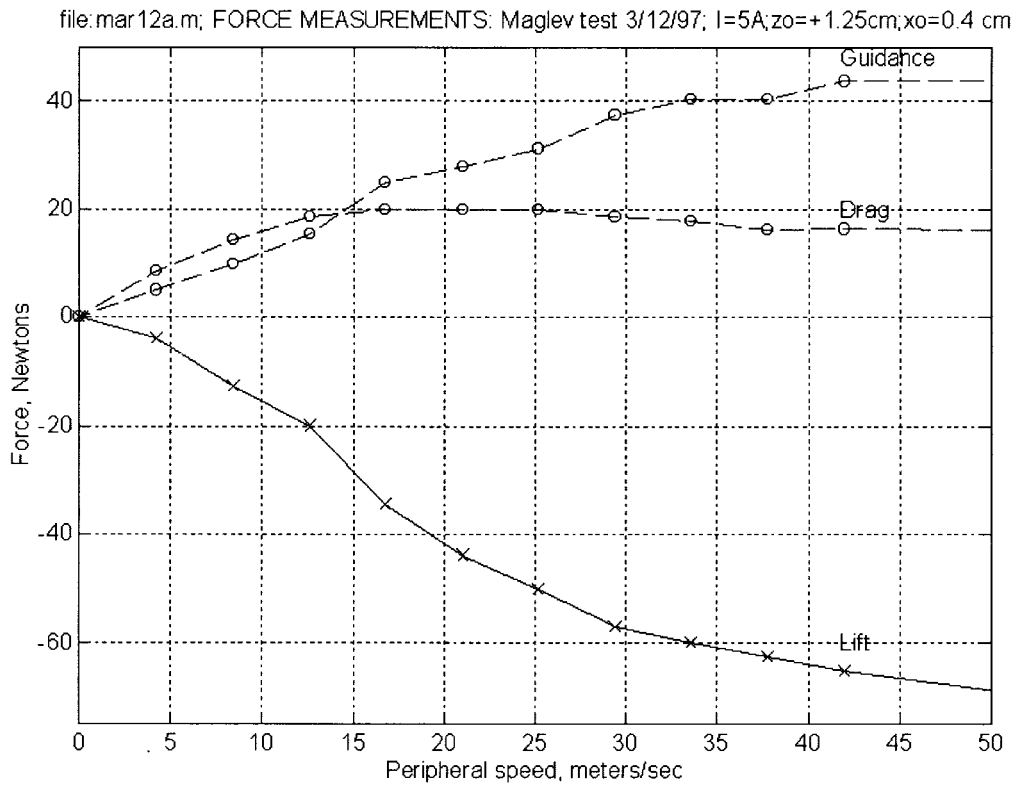
M. T. Thompson was with the Laboratory for Electromagnetic and Electronic Systems, Massachusetts Institute of Technology, Cambridge, MA 02139 USA. He is now at 25 Commonwealth Road, Watertown, MA, 02472 USA (e-mail: marctt@aol.com) and with Worcester Polytechnic Institute, Worcester, MA 01609 USA.

R. D. Thornton was with the Department of Electrical Engineering and Computer Science, Massachusetts Institute of Technology, Cambridge, MA 02139 USA. He is now with Magnemotion, Inc., Sudbury, MA 02776 USA (e-mail: mmi-rdt@magnemotion.com).

Publisher Item Identifier S 0018-9464(99)02791-0.



(a)



(b)

Fig. 1. Lift, drag, and guidance force measurements.  $I = 5$  A per coil,  $NI = 2750$  A turns per coil, all eight coils energized. (a) Magnet below null position at  $z = -0.4$  cm. (b) Magnet above null position at  $z = 1.45$  cm.

The result of calculation based on the electrodynamic models described previously is shown in Fig. 2 and compared to measured data taken with the test wheel in the range 0–600 RPM (0–50 m/s). There is good agreement for the 15-coil model for the lift force  $f_z$  and the drag force  $f_y$ . The simple

circuit model predicts a drag peak velocity of approximately 15 m/s, while the measured drag peak is approximately 20–25 m/s. The accuracy of the drag force can be further improved by accounting for parasitic eddy currents in the guideway rim, effects that are not considered by the circuit model.

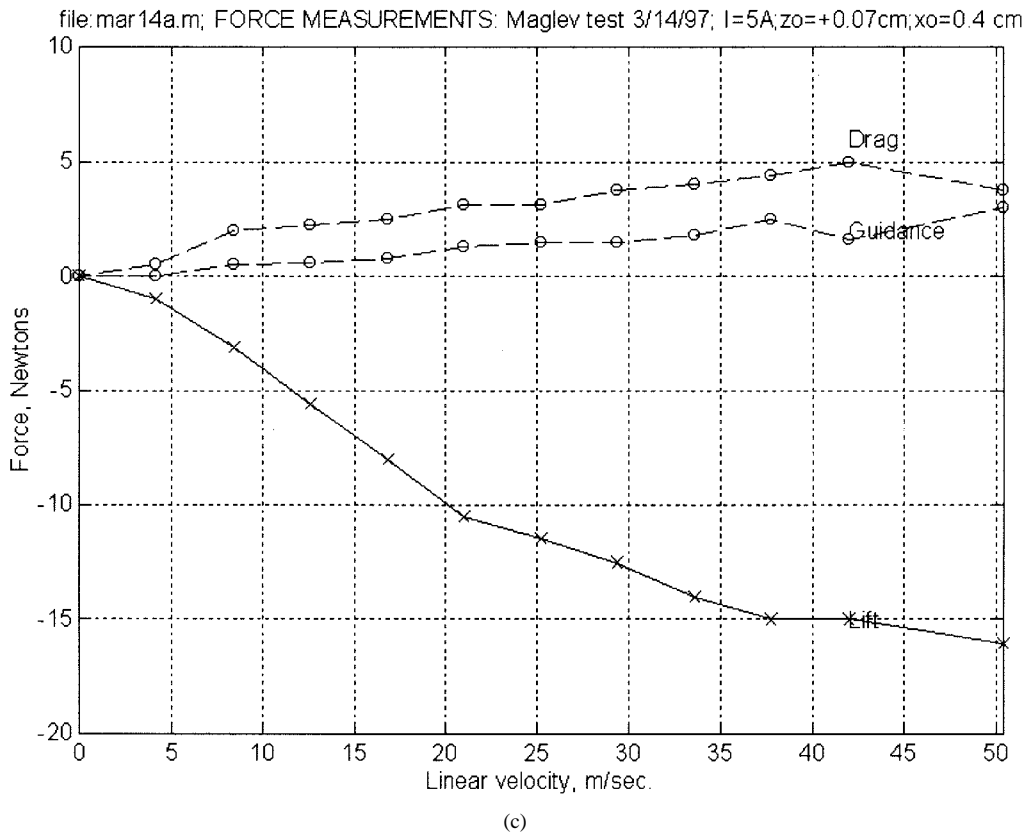


Fig. 1. (Continued). Lift, drag, and guidance force measurements.  $I = 5$  A per coil,  $NI = 2750$  A turns per coil, all eight coils energized. (c) Magnet slightly above null position at  $z = 0.27$  cm.

Referring to Fig. 2, the excitation vector (top left) is approximately a half sinusoid, corresponding to the applied magnetic field integrated over the area of the guideway loops. The shape of this excitation vector insures that only the first and second natural modes will be excited. Measurements on drag force (bottom right) bear this out, as the measured drag peak velocity was approximately 25 m/s and the electrodynamic model predicts  $\sim 40$  m/s. Higher-order modes are at significantly higher natural frequencies.

The lift force model shows good agreement with experiment in the 0–50 m/s range, although there is divergence at higher velocities. This may be due to the effects of higher-order modes at higher frequencies, but further study is warranted.

### III. THE PROBLEM OF RIDE QUALITY CONTROL

The problem of stability has long been recognized as one of the fundamental design challenges for the successful commercialization of electrodynamic maglev. The stability of maglev vehicles is of considerable interest due to its effects on passenger safety and structural requirements. Many theoretical and several experimental studies have been done to illustrate this problem.

Woods *et al.* [5] considered the stability of a levitated superconducting current ring and evaluated passive damping techniques as well as active stabilization. Davis and Wilkie [6], Fink and Hobrecht [7], and Reitz and Davis [8] studied the problem of infinitely-long wires traveling over an infinite con-

ducting sheet and found vertical and transitional instabilities in the absence of air drag.

This problem of negative magnetic damping was studied by Yamada, Iwamoto *et al.*, [9], [10] who built an experimental facility in 1973. A ferrite magnet was suspended and allowed to vibrate near a rotating aluminum drum. The damping behavior of the system was observed at various operating speeds, and it was found that negative damping exists for linear velocities above a critical velocity. For a full-scale train traveling over a sheet guideway, these results extrapolated to negative damping for train speeds higher than  $\sim 60$  km/h.

Iwasa [11] and later Iwamoto *et al.* [10] applied the impedance-modeling method to predict lift and drag forces and to study the static and dynamic stability of various vehicle-guideway configurations. Iwamoto predicts a negative damping coefficient for train speeds over  $\sim 50$  m/s traveling over a trace with discrete loops. Iwamoto recommends using passive damping to achieve good ride quality.

The conclusion of many of these early studies was that some form of damping is needed for acceptable ride quality, even in the presence of aerodynamic drag. Passive damping devices were considered, but the use of conducting plates or tuned coils between the lift magnets and the sheet guideway did not provide sufficient damping for the expected guideway roughness. It was concluded that some sort of secondary suspension or active control is needed.

The MIT team of Kolm, Thornton, Brown and Iwasa [12] studied the stability of the EDS magneplane system

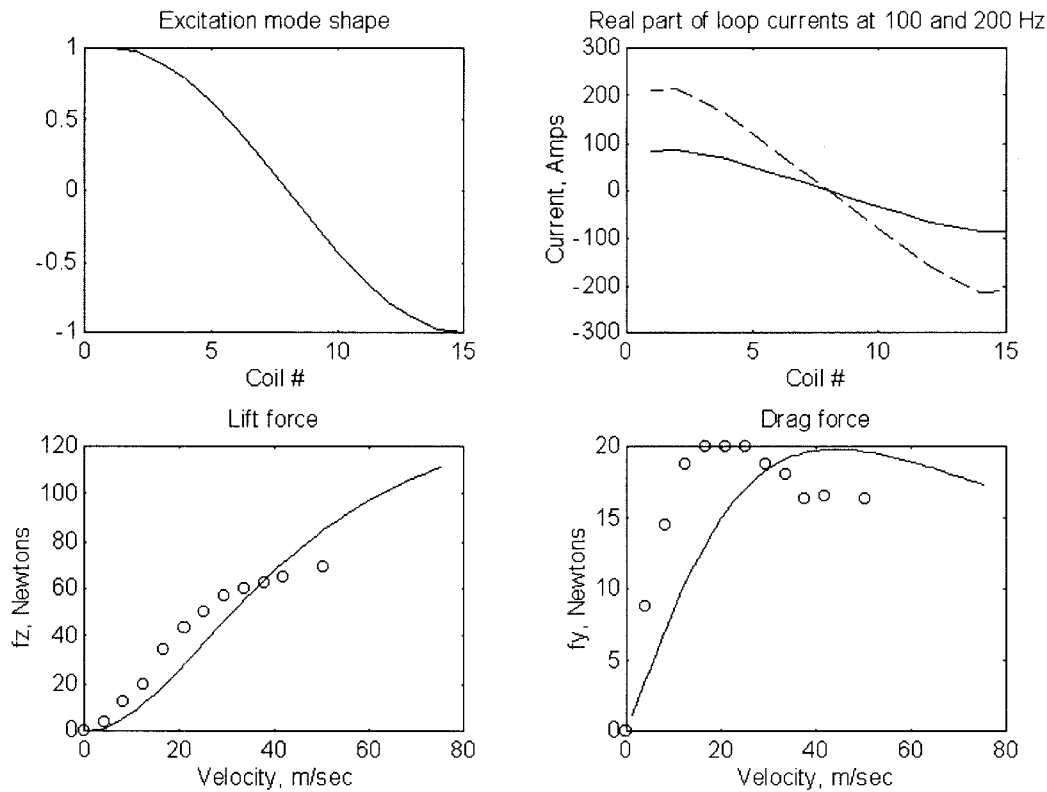


Fig. 2. Predictions of electrodynamic model with magnet +1.25 cm above null position. Upper left, coil excitation vector  $\{v\}$ ; upper right, induced loop currents  $\{I\}$  at 100 and 200 Hz. Lower left, comparison of measured to calculated lift force versus velocity; lower right, comparison of measured and calculated drag force versus velocity.

with a 1/25th-scale model and found the suspension to be underdamped and prone to catastrophic accelerations. One important development for vertical control was the use of the linear synchronous motor for heave damping.

Later stability studies have focused on dynamic instabilities and the effects of mode coupling. Chu and Moon [13], demonstrated instabilities in a two degrees-of-freedom (D.O.F.) electrodynamic maglev model, showing limit cycle oscillations at operating speeds near the maglev drag peak. Due to the small scale of their model, aerodynamics significantly affected their results. In other experiments, Moon [14] reports results from a rotating wheel test facility for study of lateral, heave, roll, yaw, and pitch motions. A yaw-roll instability was observed.

The most detailed study of instabilities to date in EDS maglev has been performed by the maglev group at the Argonne National Laboratory [15], [16]. Suspension instabilities of EDS systems with three and give degrees of freedom (D.O.F.) have been evaluated by computer simulation. Their results show that coupling effects among the five D.O.F. play an important role and that there are several potential instabilities. The instabilities depend on the equilibrium air gap, which in turn is determined by the vehicle mass, passenger load, and guideway design.

An active secondary suspension using high-temperature superconductors has been built and analyzed by the MIT group of Thornton and Thompson with help from Kondoleon and Draper Laboratory [1]–[4]. With scaling law studies and tests on a rotating test wheel facility, it was shown that it is possible

to actively control the magnet position to achieve good ride quality with reasonable levels of power and energy from the control source.

It should be noted that many of the reported instabilities are related to the propulsion means. If a constant propulsive force is used, instability can arise because the magnetic drag decreases with increasing speed. In many cases the use of a constant speed propulsion, or the use of feedback control for the linear motor, would eliminate the instability.

#### A. Active Magnetic Suspension

A controllable magnetic primary suspension has a big advantage over an uncontrolled primary suspension combined with an active mechanical secondary suspension: the magnetic force acts directly on the guideway and does not require that there be any “unsprung” weight. EMS systems have the same advantage, but the air gap is so small that an active primary suspension has not been deemed sufficient to give adequate ride quality at high speeds. In 1972 an MIT research project demonstrated the ability of a linear synchronous motor (LSM) to produce controllable vertical forces on a maglev vehicle, and this allowed the damping of heave motion [17]. By mounting the LSM in different configurations it is possible to counteract sway as well as heave, but since the force acts uniformly over the whole vehicle it is not possible to control pitch or yaw. Therefore, additional magnetic forces are needed to augment the LSM forces.

In principal one could directly control the current in the vehicles suspension magnets, but this is impractical because

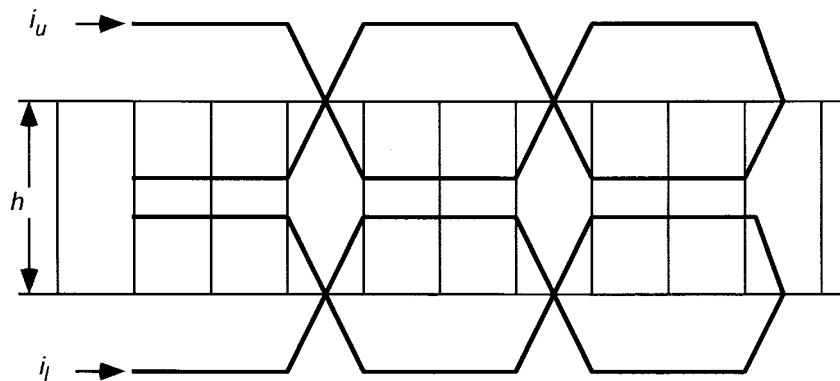


Fig. 3. Simplified flux canceling suspension.

of the large energy storage associated with these magnets. This is particularly true of the most common design which uses a single array of low temperature superconducting coils without any ferromagnetic material in the flux path. Such designs have large external fields with a very large magnetic energy storage, and this energy must be changed relatively fast to provide good ride quality. Moreover, the low temperature superconducting wire can not tolerate large ac components of current and magnetic field without quenching.

The design reported here incorporates three features, each of which contributes to making it feasible to construct a controllable magnetic suspension.

- The vehicle magnets use high temperature superconducting wire that is able to tolerate substantial ac current without excessive power loss.
- The vehicle magnets use an iron core which greatly reduces the amount of energy stored in the field.
- The suspension uses the flux canceling design for which a small differential magnetic field can produce a significant force.

Taken together, these features make it possible to have a reasonable amount of power control the ride quality for a suspension that can tolerate several centimeters of vertical motion.

### B. Simplified Control Model of "Flux-Canceling" Suspension

Prior publications and a companion paper in these TRANSACTIONS [1]–[4], [18] provide a detailed description of the "flux-canceling" suspension system, but for this paper we use the simpler model shown in Fig. 3. This figure represents the vehicle magnets by two wave windings and the guideway by a simple ladder. Each vehicle has two identical suspension systems, one on each side of the vehicle. The guideway can be a channel, with the guideway ladder mounted on the inside vertical walls of the channel, or the guideway can be a monorail, with the guideway ladder mounted on the outside of the monorail. The suspension forces are shear forces between the guideway and vehicle and any lateral forces are balanced by lateral forces on a separate suspension system on the other side of the vehicle. For this paper we only consider the suspension forces for a single system. The same ideas can be applied to control guidance forces, but guidance is not discussed in this paper.

The heavier lines show the ends of two wave windings and the lighter lines show a guideway ladder. The two structures are laterally displaced by a distance that is much less than  $h$ , the height of the ladder. The actual vehicle magnets consist of windings on the poles of a ferromagnetic structure and the guideway uses more vertical members and a more elaborate arrangement in order to minimize unwanted eddy currents, but this simple model is adequate for the analysis of an active suspension system. The analysis assumes the vehicle is moving with respect to the guideway, so there is the potential for the vehicle to induce ac currents in the guideway and thereby produce vertical lift forces on the vehicle.

The lower and upper magnet currents are labeled  $i_l$  and  $i_u$ . Assuming these two currents are constant and equal, if the vehicle coils are vertically centered with respect to the guideway ladder, then there is no induced current in the ladder and no force on the vehicle. If the vehicle is displaced either up or down, then there is an induced current that creates a restoring force; i.e., the suspension behaves like a magnetic spring. Note that even though there is considerable power loss in the guideway ladder, the suspension is undamped except for minor losses due to aerodynamic effects and eddy currents that are not represented in this simplified model.

The key to the analysis is to note the functional dependence of vertical force on currents. Although the currents in the rung and side elements in the ladder have a complex behavior, we can imagine a composite RMS current, called  $i_g$ , that characterizes the behavior. In order to simplify the analysis define sum and difference values of the vehicle coil currents. The sum  $i_s$  is the suspension current that is used to control the equilibrium position and the difference  $i_c$  is the control current that is used to control ride quality

$$\begin{aligned} i_s &= i_l + i_u \\ i_c &= i_l - i_u. \end{aligned} \quad (1)$$

If the vehicle is going fast enough to be on the high speed side of the drag peak, then we can express the effective guideway current as

$$i_g = k_1(i_s y + i_c h_e) \quad (2)$$

where  $k_1$  is a proportionality constant that depends on many details of the design,  $y$  is the vertical displacement of the vehicle from equilibrium, and  $h_e$  is an effective height that

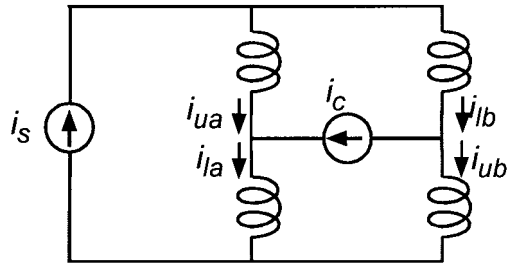


Fig. 4. Bridge connection of vehicle windings.

determines the induced voltage; in a typical design  $h_e$  is about  $0.4h$ , where  $h$  is the height of the guideway as shown in Fig. 3.

Given  $i_g$  we can express the vertical lift force  $F_y$  as

$$F_y = k_2 i_g i_s \quad (3)$$

where  $k_2$  is another proportionality constant that depends on the design details.

Define  $y_0$  as the displacement  $y$  at equilibrium when the vertical force equals the weight of the vehicle  $mg$ . Then, combining (1)–(3) we have

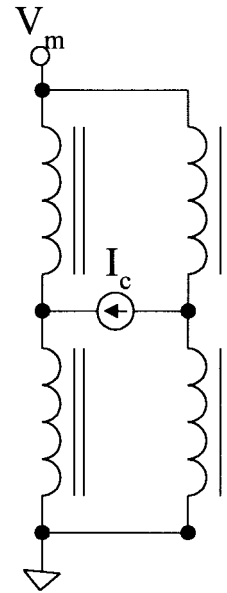
$$F_y = mg \left( 1 + \frac{i_c h_e}{i_s y_0} \right). \quad (4)$$

We interpret (4) as follows. If we wish to exert a control force, say a controllable force up to 0.2 g, then we need to make the second term in parenthesis in (4) have a value of up to 0.2. For a typical full scale design  $h_e = 0.2$  m and  $y_0 = 0.1$  m, the control current needs to be only about 10% as large as the suspension current. This 0.2 g of control force is in addition to any force produced by the LSM, which can also be on the order of 0.2 g, either up or down. Since the vehicle is suspended by a long array of magnets, each can have its own control system, exactly as with EMS designs. Then it is possible to provide controllable pitch forces, and if the same ideas are applied to guidance it is possible to produce controllable yaw forces.

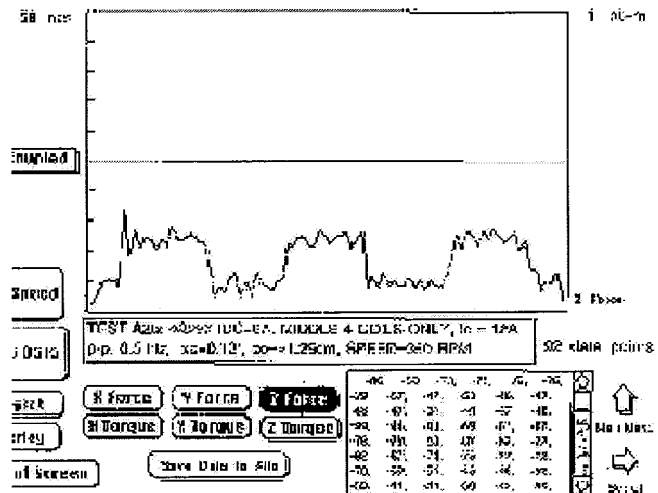
In order to control the ride quality we separate each of the wave windings in Fig. 3 into two equal parts and connect them in the bridge configuration shown in Fig. 4.

The suspension current  $i_s$  excites the bridge so as to control the sum of the magnet currents and the control current  $i_c$  excites the bridge so as to control the difference of the magnet currents. In this way we have a simple way to provide only the differential current required for ride quality control.

An important point to note is that there are mutual inductances between the various coils in Fig. 4, and the inductance seen by the suspension current source is typically about twice as large as the inductance seen by the control current. This reduction in control circuit inductance reduces still further the power and energy needs to effect ride quality control. In short, it takes less than 1% as much energy to effect a 0.2 g control force as it does to provide the equilibrium suspension force. For a typical design the power and energy required for good ride quality can be less than the power and energy required to control the magnets in an EMS system.



(a)

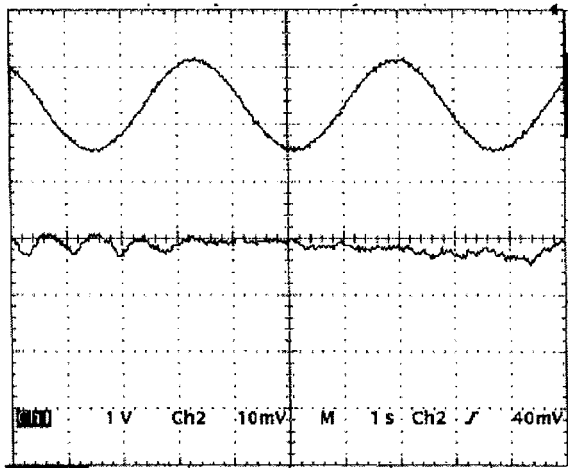


(b)

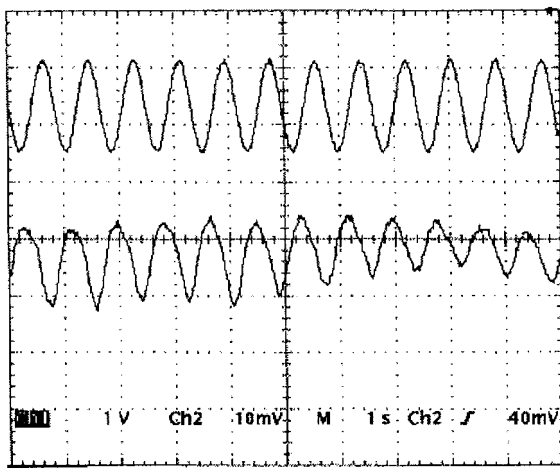
Fig. 5. Differential lift measurement. (a) Magnet wiring for differential lift measurement. (b) Magnet driven with square wave of control current. Lift force measurement, dc current = 6 amps/coil, control current = 12 amp square wave at 0.5 Hz.

### C. Active Secondary Magnetic Suspension Test Results

In order to test the concept of varying the lift force by using differential current control, a control current source was connected as in Fig. 5(a). The test wheel was run at 350 RPM. Each of the coils was energized with six amps dc by the main power supply  $V_m$ . A 12-amp peak-to-peak square wave driven by the control current source  $I_c$  and the resultant measured lift force is shown Fig. 5(b). The magnet was set above the null position, and hence the average lift force is negative. This test verifies that it is possible to control the vertical force by controlling the magnet nodes shown in the figure. The advantage of driving at these points is that the effective inductance at the coil terminals is decreased by mutual coupling between magnet coils.



(a)

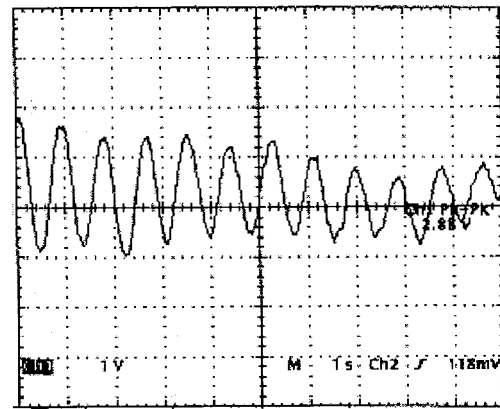


(b)

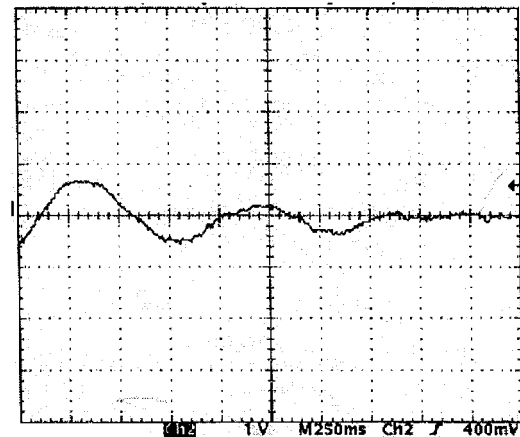
Fig. 6. Vertical vibration test; system driven with sinusoidal current at differential drive terminals. (a) Magnet driven well below resonance. Top trace: magnet current, 5 amps/div. Bottom trace: magnet vertical deflection, 1 cm/div. (b) Magnet driven near resonant frequency  $f = 1.15$  Hz. Top trace: magnet current, 5 amps/div. Bottom trace: magnet vertical deflection, 1 cm/div.

In a follow-up experiment, the magnet was mounted to a one-DOF air bearing which allowed low-friction vertical vibration of the magnet while the suspension was energized with dc current. The magnet was allowed to bounce freely at its vertical natural frequency. The dc current for these tests was set to 5 A, the test wheel was set to 350 RPM (30 m/s peripheral speed), and an underdamped vertical natural frequency of 1.15 Hz was measured. In Fig. 6(a), the differential control terminals are driven with a 12 A peak-to-peak (p-p), 0.2 Hz sinusoidal current signal. The bottom trace shows little motion, as the magnet is driven well below the resonant frequency. In Fig. 6(b), the magnet is driven with a sinusoidal current at 1.1 Hz, near the measured resonant frequency. As expected, there is significant vertical deflection of the magnet as the suspension is driven near resonance.

With the air bearing energized and the control system deactivated, the vertical magnet position was perturbed approximately +1 cm from the equilibrium position and the resultant transient decay of magnet position was observed



(a)



(b)

Fig. 7. Performance of active secondary magnetic suspension. (a) Control system not operating. Initial deflection  $\sim 1$  cm; magnet bounces at EDS natural frequency 1.15 Hz. (b) Active damping enabled, using PID controller, damping ratio  $\sim 40\%$ . (Note change in time scale.)

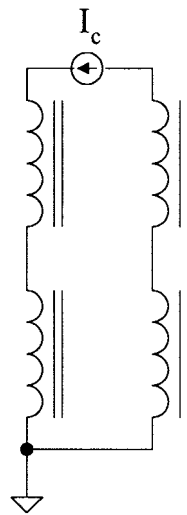
[Fig. 7(a)]. The oscillation frequency is at 1.15 Hz with a damping ratio of approximately 1%, corresponding to the expected underdamped EDS response.

A similar experiment was run, but with the control system operating with a simple proportional-integral-derivative controller [Fig. 7(b)]. The resultant magnet vertical position response is much more damped ( $\zeta \sim 40\%$ ) showing that the control system is operating correctly. Further improvement can be made in the transient response by adjusting the loop parameters. This test shows that it is possible to use an active secondary magnetic suspension for ride quality control with this geometry.

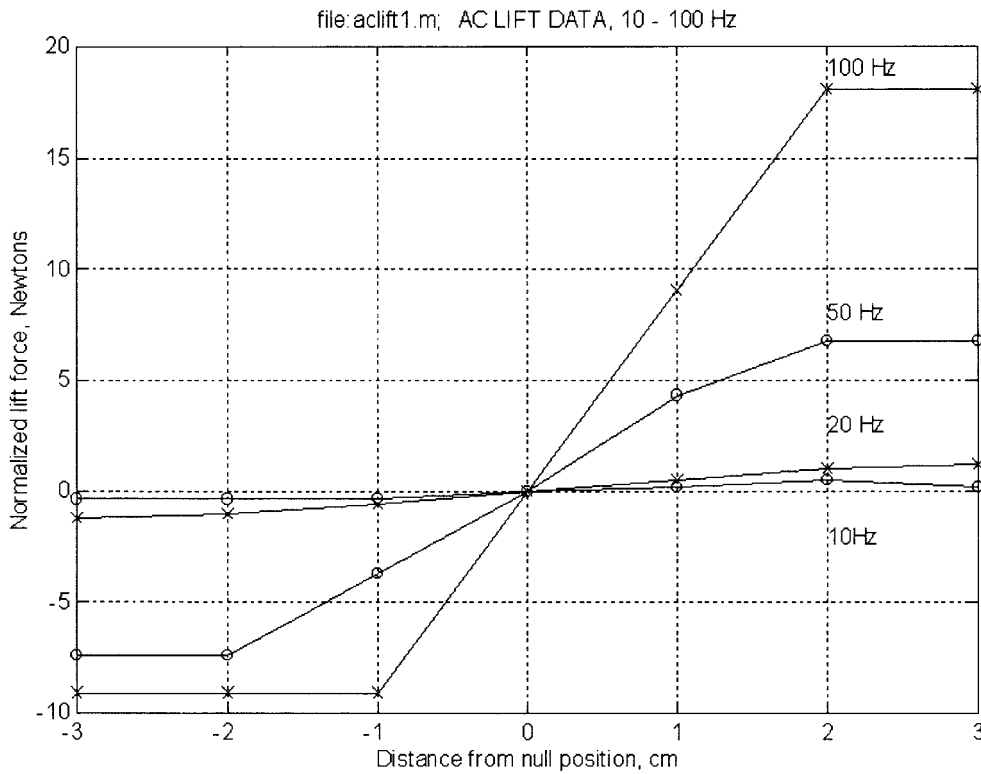
#### IV. ZERO-VELOCITY LIFT

Further tests were run to determine if significant lift is possible at zero train velocity by exciting the levitation coils with ac currents. Generating lift at zero velocity is desirable, as this can remove the need for a low speed suspension. The fact that high temperature superconductors are robust with regard to ac losses is a further motivation, as such control is difficult using low temperature superconductors due to quenching.

For this series of tests, the coils were wired as in Fig. 8(a). The coils were wired so that for the first half cycle of the



(a)



(b)

Fig. 8. “Zero velocity” lift measurements at 10, 20, 50, and 100 Hz. (a) Magnet wiring and (b) test results.

sinewave current excitation, the top two coils are in a North-North arrangement, and the bottom two coils are energized South-South. For this configuration, if the guideway is offset from the null position, there is a net changing flux through the guideway loops and hence a restoring force.

Results of ac lift measurements are shown in Fig. 8(b) for various equilibrium displacements from the null position and for excitation frequencies of 10, 20, 50, and 100 Hz. A maximum frequency of 100 Hz was chosen<sup>1</sup> as this is the

<sup>1</sup> If the operating frequency is known and does not change a series capacitor can be added to resonate with the inductive load to reduce the large reactive voltage required to drive the magnet coil.

approximate equivalent frequency of the maglev drag peak, and higher frequencies will not result in significantly higher lift. The data shows that lift comparable to that achieved by electromagnetic induction by motion can be achieved, however at the cost of high power delivery from the magnet current source. In a full-scale suspension, “zero velocity lift” would be energized for a few seconds as the train leaves the station. After EDS lift off, the ac current would be deactivated.

#### V. DEVELOPMENT OF EDS MAGLEV SCALING LAWS

The goal of this section is to predict performance of a full-scale maglev system based on scaling laws, simple guideway

TABLE I  
SCALING LAW SUMMARY FOR EDS MAGLEV SCALED BY FACTOR  $\ell$  PRIMED COORDINATES ARE FOR THE SCALED-UP SYSTEM

<i>Parameter</i>	<i>Constitutive Relation</i>	<i>Scaling law</i>
Guideway loop self-inductance, $L$	$L \propto \ell PF$	$L' = \ell L$
Guideway loop self-resistance, $R$	$R \propto 1/\sigma \ell$	$R' = R/\ell$
Guideway dominant time constant, $\tau$	$= L/R \propto 1/\ell^2$	$\tau' = \tau \ell^2$
Effective frequency at guideway, $\omega$		$\omega' = \omega/\ell$
Drag peak velocity		$v_{pk}' = v_{pk}/\ell$
$N$ , turns	$\propto \ell^2$	$N' = \ell^2 N$
Average field normal to guideway, $B_o$	$\propto NI/\ell \propto \ell$	$B_o' = \ell B_o$
Induced guideway loop voltage, $V_i$	$\propto j\omega B_o \ell^2 \propto \ell^2$	$V_i' = \ell^2 V_i$
Max. induced loop current, $I_i$	$\propto V_i/j\omega L \propto \ell^2$	$I_i' = \ell^2 I_i$
Lift force at cruising speed, $f_z$	$\propto B_o I_i \ell \propto \ell^4$	$\propto B_o I_i \ell \propto \ell^4$
Drag force at high speed, $f_y$	$\propto I_i^2 R \propto \ell^2$	$\propto I_i^2 R \propto \ell^2$
Lift/drag ratio at drag peak speed	$= f_z/f_y$	$\propto \ell$

coil geometries, and test results from the 1/5 scale-model magnet. Results may be extrapolated from calculations on simple resistance-inductance circuits, as the previously mentioned measurements have proven this approximate technique to be valid. It is assumed that in scaling up the system, every linear dimension in the guideway and magnet is scaled by the factor  $\ell$ . This analysis does not consider second-order effects, such as increased eddy current losses.

As shown previously, the inductance of a disk inductor has the form

$$L \propto aPF \quad (5)$$

where  $a$  is the mean coil radius. If all dimensions of the inductor are scaled by the factor  $\ell$ , the inductance also scales by the same factor as  $P$  and  $F$  remain constant. The self-resistance of the loop is given by

$$R \approx \frac{2\pi a}{\sigma bc} \quad (6)$$

and this resistance scales as  $1/\ell$ . The resultant time constant of the loop (given by  $L/R$ ) scales as  $\ell^2$  and shows that large-scale inductors are more efficient than small ones. This is equivalent to stating that the low frequency  $Q$  (i.e., the non skin depth limited) is higher for large inductors. Given this scaling, the EDS drag peak velocity is expected to scale as  $1/\ell$  (as the effective guideway frequency  $\omega$  scales as  $1/\ell$ ), although the effects of parasitic eddy currents will modify this somewhat.

The number of coil turns ( $N$ ) scales with the winding area, or as  $\ell^2$ . The average guideway field scales as  $\ell$ , due to the  $\ell^2$  factor increase in turns, and the  $\ell$  increase in pole pitch. The induced voltage  $V_i$  around a guideway loop may be expressed

as

$$V_i = j\omega B_o A \propto \ell^2 \quad (7)$$

where  $B_o$  is the average magnetic field, and  $A$  is the area of the guideway loop. In the high-speed limit, the induced current is limited by the inductance of the coil, as

$$I_i \approx \frac{V_i}{j\omega L} \propto \ell^2. \quad (8)$$

The lift force is due to the product of the induced current, the applied magnetic field, and the length scale, or

$$f_z \propto I_i B_o \ell \propto \ell^4. \quad (9)$$

The maximum lift force scales as  $\ell^4$ , which could also be inferred from evaluating the magnetic pressure acting on the iron polefaces (where  $B_o$  scales as  $\ell$  and area scales as  $\ell^2$ ). The drag force scales as  $I_i^2 R$  or as  $\ell^2$  and hence the lift/drag ratio at the drag peak speed scales as  $\ell$ . Other parameters such as scaling of lift/drag and lift-to-weight ratio may also be inferred from the test results. A summary of the scaling laws is shown in Table I.

Using these scaling laws, performance of a full-scale magnet based on copper coils and on HTSC coils operating at 40 K has been predicted (Table II). The extrapolation from our 1/5-scale test results to 1.0 scale copper and for copper operating at 77 K is straightforward if limitations imposed by air cooling of the copper magnets are not considered. It is unlikely that the number of ampere turns shown for the full-scale copper magnet would be achieved in practice due to heat transfer. Also, it is unlikely that the high lift-to-drag ratios at 100 m/s would be achieved in practice due to high eddy current losses (made worse by the larger geometry).

TABLE II  
SCALING LAW SUMMARY APPLIED TO TEST DATA. COMPARISON BETWEEN 1/5 SCALE SUSPENSION TEST RESULTS, 1.0-SCALE COPPER MAGNET OPERATING AT ROOM TEMPERATURE, 1.0 SCALE COPPER AT 77 K, AND HTSC AT 40 K. (COOLING WEIGHT NOT INCLUDED)

<i>Parameter</i>	<i>1/5-scale</i>	<i>1.0 scale</i>	<i>1.0 scale</i>	<i>HTSC</i>
	<i>model</i>	<i>copper</i>	<i>copper, 77K</i>	<i>@ 40K</i>
Guideway loop self-inductance, $L$	280 nH	1.4 $\mu$ H	1.4 $\mu$ H	1.4 $\mu$ H
Guideway loop self-resistance, $R$	0.0007 $\Omega$	0.00014 $\Omega$	0.00014 $\Omega$	0.00014 $\Omega$
Loop time constant, $\tau$	0.4 msec	10 msec	10 msec	10 msec
Levitation coil turns, $N$	550 turns	13750	13750	1500
Levitating coil operating current, $I$	5 Amps	5	14.4	136 <sup>1</sup>
Levitation power dissipation	680 Watts	85 kW	85 kW	0
$NI$ , each coil	2750 A-turn	68750	198,450	198,450
Current density in winding, $\lambda J$	275 A/cm <sup>2</sup>	275	800	7500
Average field normal to guideway, $B_D$	0.067 Tesla	0.335	0.96	0.96
Lift force at $v = 100$ m/s, $f_z$	70 Newtons	43.8 kN	365 kN	365 kN
Drag force at drag peak, $f_y$	20 Newtons	2.5 kN	20.8 kN	20.8 kN
Drag peak velocity $v_{pk}$	25 m/sec	5 m/sec.	5 m/sec.	5 m/sec.
Drag force at $v = 100$ m/sec	9.4 N	249 N	2.1 kN	2.1 kN
Lift/drag ratio at $v = 100$ m/s	7.4	175	175	175
Magnet core weight	29 kg	3625	3625	3625
Coil weight	8 kg	1000	1000	106
Total magnet weight <sup>2</sup>	37 kg	4625	4625	3731
Magnetic drag power @ 100 m/sec	0.94 kW	24.9 kW	208 kW	208 kW
Guideway power, kW/ton of lift	120 kW/ton	5.07	5.07	5.07
Lift/weight ratio	0.19	0.97	8.0	10.0

It is assumed that the copper coils operating at 77 K have the same power dissipation as 1.0-scale copper coils operating at room temperature. Therefore, a higher coil current is possible at 77 K since the conductivity of copper at liquid nitrogen temperature is only 13% of the room temperature value. This assumes that there is sufficient copper area exposed to the boiling liquid nitrogen. An upper limitation<sup>2</sup> for allowable power dissipation in the copper coil is the peak nucleate boiling heat transfer flux, which for liquid nitrogen is  $q_{pk} \sim 15$  watts/cm<sup>2</sup> [19, p. 113].

The performance of a silver-sheathed HTSC magnet operating at 40 K is extrapolated from the copper coil results and from available data taken from tests on HTSC coils and samples of HTSC tape. The achievable current density in HTSC at 40 K is much higher than that in HTSC at 77 K

<sup>2</sup>Assuming that the winding has sufficient ventilation space for the liquid nitrogen to vent.

(approximately by a factor of 2–6 from published data). For the same number of ampere turns, less material will be needed for the HTSC design, resulting in a lighter coil. Current HTSC tapes are available with critical current  $I_c = 40$  A at 77 K corresponding to a critical current density significantly higher than that supported by copper at 77 K. A value of  $I = 100$  A or higher seems reasonable for an HTSC coil design at 40 K given current technology [20]. Further improvement may be made by adjusting the dimensions of the core, as the full winding area will not be needed.

The performance of the predicted 1.0-scale HTSC magnet at 40 K is comparable to that of the Japanese MLU002 test vehicle, which operates with an magnetomotive force of 700 kA turns while generating a levitating force of 196 kiloNewtons [21, p. 7]. The advantage to the iron-core HTSC design is that less Ampere turns and less superconducting material is needed, and there is the possibility of actively

TABLE III  
SCALING LAWS APPLIED TO AC LIFT MEASUREMENTS (CRYOSTAT WEIGHT NOT INCLUDED)

	<i>1/5-scale copper, I = 12A, 100 Hz</i>	<i>1.0 scale HTSC @ 40K, I=80A p-p, 100 Hz</i>	<i>1.0 scale HTSC @ 40K, I=240A p-p, 100 Hz</i>
Ampere turns, p-p	6,600	165,000	495,000
Lift force	17 N	10625 N	95,625 N
Lift/weight ratio	0.05	0.28	2.5

controlling the magnet currents to achieve acceptable ride quality.

For "zero-velocity lift" scaling laws can be used to show that a full-scale magnet with eight coils each with  $NI = 165\,000$  (corresponding to  $N = 2062$  turns and  $I = 80$  A p-p) will generate approximately 1 ton of lift with a lift-to-weight ratio of 0.28 at 100 Hz (Table III). With  $NI = 495\,000$  A turns p-p, a magnet lift-to-weight ratio of  $\sim 2.5$  will be achieved for a full-scale magnet based on an HTSC coil. The primary losses will be switching losses in the driving electronics and ac losses in the levitation and guideway coils. The actual lift-to-weight ratio will be less due to the weight of the cooling system, and further study is required to determine the extent of power losses in the HTSC coil due to switching.

## VI. CONCLUSIONS

Results from these series of maglev tests show that there is good agreement between predictions based on simple circuit models with measurements taken on the test fixture for lift force, drag force, and magnetic drag peak. The models could be improved by doing additional finite-element analyses and extending the 15-coil model so that the infinitely long guideway is better approximated.

The use of an iron core offers significant advantages such as rapid attenuation of the far magnetic field. Furthermore, the iron core reduces the mass of superconducting material needed for a given guideway field. The iron can be used to reduce the magnetic field impinging on the coils so that the critical current is maximized.

Vertical force can be controlled by differential control of the magnet currents. Vertical position can be actively damped by utilizing an active magnetic secondary suspension. Use of HTSC may overcome the limitations imposed by mechanical secondary suspensions. The guidance force measured was a significant fraction of the lift force. Similar reasoning could be used to design a guidance system, for horizontal train control, based on flux-canceling concepts.

It is possible to generate lift with ac currents using this configuration. The robustness of HTSC with regard to ac losses may make ac lift a viable alternative to low-speed mechanical suspensions. However, cooling requirements will probably limit the duration for which ac lift may be operated. Scaling laws were derived which show that the performance of an HTSC-based design at 40 K may be comparable to that of low-temperature superconducting designs, with the advantage

of less weight and the possibility of using ac lift for low-speed suspension.

## ACKNOWLEDGMENT

The authors gratefully acknowledge the support of the Laboratory for Electromagnetic and Electronic Systems and the Center for Transportation Studies at the Massachusetts Institute of Technology, the U.S. Department of Transportation under the Federal Railway Administration, and the Charles Stark Draper Laboratory, who provided research support.

## REFERENCES

- [1] A. Kondoleon, D. Seltzer, R. D. Thornton, and M. T. Thompson, "Development of a large scale high speed wheel test facility," in *Proc. 3rd Int. Symp. Magn. Suspension Technol.*, Tallahassee, FL, NASA Conf. Publ. 3336, pt. 2, pp. 523-534, Dec. 13-15, 1995.
- [2] M. T. Thompson, "High temperature superconducting magnetic suspension for maglev," Ph.D. dissertation, Dep. Elect. Eng. Comput. Sci., Massachusetts Institute of Technology, Cambridge, MA, May 1997.
- [3] M. T. Thompson and R. D. Thornton, "Modeling of HTSC based iron-core flux-canceling electrodynamic suspension for maglev," in *Proc. 4th Int. Symp. Magn. Suspension Technol.*, NASA Conf. Publ., Gifu, Jpn., 1997, submitted for publication.
- [4] R. D. Thornton and M. T. Thompson, "Magnetically based ride quality control for an electrodynamic maglev suspension," in *Proc. 4th Int. Symp. Magn. Suspension Technol.*, Gifu, Jpn., NASA Conf. Publ., 1997.
- [5] C. H. Woods, R. K. Cooper, V. K. Neil, and C. E. Taylor, "Stability analysis of a levitated superconducting current ring stabilized by feedback and eddy currents," *J. Appl. Phys.*, vol. 41, no. 8, pp. 3295-3305, July 1970.
- [6] L. C. Davis and D. F. Wilkie, "Analysis of motion of magnetic levitation systems: Implications for high-speed vehicles," *J. Appl. Phys.*, vol. 42, no. 12, pp. 4779-4793, Nov. 1971.
- [7] H. J. Fink and C. E. Hobrecht, "Instability of vehicles levitated by eddy current repulsion—Case of an infinitely long current loop," *J. Appl. Phys.*, vol. 42, no. 9, pp. 3446-3450, Aug. 1971.
- [8] J. R. Reitz and L. C. Davis, "Force on a rectangular coil moving above a conducting slab," *J. Appl. Phys.*, vol. 43, no. 4, pp. 1547-1553, Apr. 1972.
- [9] T. Yamada, M. Iwamoto, and T. Ito, "Magnetic damping force in inductive magnetic levitation system for high-speed trains," *Elec. Eng. (Japan)*, vol. 94, no. 1, pp. 80-84, 1974.
- [10] M. Iwamoto, T. Yamada, and E. Ohno, "Magnetic damping force in electrostatically suspended trains," *IEEE Trans. Magn.*, vol. MAG-10, pp. 458-461, May 1974.
- [11] Y. Iwasa, "Electromagnetic flight stability by model impedance simulation," *J. Appl. Phys.*, vol. 44, no. 2, pp. 858-862, Feb. 1973.
- [12] H. H. Kolm, R. D. Thornton, Y. Iwasa, and W. Brown, "The magneplane system," *Cryogenics*, pp. 377-384, July 1975.
- [13] D. Chu and F. C. Moon, "Dynamic instabilities in magnetically levitated models," *J. Appl. Phys.*, vol. 54, no. 3, pp. 1619-1625, Mar. 1983.
- [14] F. C. Moon, "Vibration problems in magnetic levitation and propulsion," *Transport Without Wheels*, E. Laithwaite, Ed. London, U.K.: Elek Sci., 1977, pp. 122-161.
- [15] S. S. Chen, S. Zhu, and Y. Cai, "On unsteady-motion theory of magnetic forces for maglev systems," *J. Sound Vibration*, vol. 188, no. 4, pp. 529-543, 1995.

- [16] Y. Cai, D. M. Rote, T. M. Mulcahy, Z. Wang, S. S. Chen, and S. Zhu, "Dynamic stability of repulsive-force maglev suspension systems," Argonne Nat. Lab., France, Rep. ANL-96/18, Nov. 1996.
- [17] W. S. Brown, "A 1/25 scale magneplane," Ph.D. dissertation, Dep. Elec. Eng. Comput. Sci., Massachusetts Institute of Technology, Cambridge, MA, Oct. 1975.
- [18] R. D. Thornton, "Flux canceling maglev suspension," in *MAGLEV '93, Proc. 13th International Conf. Magnetically Levitated Syst. Linear Drives*, Argonne Nat. Lab., Argonne, IL, May 1993.
- [19] Y. Iwasa, *Case Studies in Superconducting Magnets*. New York: Plenum, 1994.
- [20] Y. Iwasa, personal communication, 1997.
- [21] J. L. He, D. M. Rote, and H. T. Coffey, "Study of Japanese electrodynamic-suspension maglev systems," Argonne Nat. Lab., France, Rep. ANL/ESD-20, Apr. 1994.

**Marc T. Thompson** (M'92) received the B.S.E.E. degree from the Massachusetts Institute of Technology (MIT), Cambridge, MA, in 1985, the M.S.E.E. degree in 1992, the Electrical Engineer's degree in 1994, and the Ph.D. degree in 1997.

Presently, he is an engineering consultant and Adjunct Associate Professor of Electrical Engineering at Worcester Polytechnic Institute, Worcester, MA. At Worcester Polytechnic Institute, he teaches intuitive methods for analog circuit, magnetic, thermal, and power electronics design. His main research at MIT concerned the design and test of high-temperature superconducting suspensions for maglev and the implementation of magnetically based ride quality control. Other areas of his research and consulting interest include planar magnetics, power electronics, high speed analog design, induction heating, IC packaging for improved thermal and electrical performance, use of scaling laws for electrical and magnetic design, and high speed laser diode modulation techniques. He has worked as a consultant in analog, electromechanics, mechanical, and magnetics design. He also holds two patents. Currently he works on a variety of consulting projects including high power and high speed laser diode modulation, eddy-current brake design for amusement applications, flywheel energy storage for satellites, and magnetic tracking for inter-body catheter positioning. He is a consultant for Magnemotion, Inc. and Polaroid Corporation.

**Richard D. Thornton** (S'51-A'52-M'57-SM'75-LF'94) was formerly Professor of Electrical Engineering and Computer Science at the Massachusetts Institute of Technology (MIT), Cambridge, MA, with primary research in magnetic levitation and propulsion and power electronic control systems. In addition, he teaches and is involved in research on modeling and simulation of electronic circuits and microprocessor controlled electromagnetic and electro-mechanical systems. Starting in 1965, he worked on various transportation projects in conjunction with the DOT supported MIT Project Transport. From 1970 to 1975, he worked with Dr. Henry Kolm and others at MIT on the development of the NSF supported MIT Magneplane. He is author or co-author of three international patents on the Magneplane System. He was a member of the maglev Technical Advisory Committee, reporting to the U.S. Senate. Since 1987, the main focus of his work has been on maglev suspension, linear motor propulsion, and fault tolerant control. He has written several papers and presented many talks on the design of suspension systems and multimewatt power electronic control systems. He has worked with members of the electric utility industry to study the proper design of electric power distribution systems for high speed ground transportation, and has also reviewed the research of others in this field. He is President of Magnemotion, Inc., Sudbury, MA.